PHILOSOPHICAL TRANSACTIONS A

royalsocietypublishing.org/journal/rsta

Research

Cite this article: Olivier F *et al*. 2020 Shells of the bivalve *Astarte moerchi* give new evidence of a strong pelagic-benthic coupling shift occurring since the late 1970s in the North Water polynya. *Phil. Trans. R. Soc. A* **378**: 20190353.
http://dx.doi.org/10.1098/rsta.2019.0353

Accepted: 7 April 2020

One contribution of 18 to a theme issue 'The changing Arctic Ocean: consequences for biological communities, biogeochemical processes and ecosystem functioning'.

Subject Areas:
oceanography

Keywords:
Arctic, climate change, sclerochronology, pelagic-benthic coupling, match/mismatch hypothesis, bivalve growth

Author for correspondence:
Frédéric Olivier
e-mail: frederic.olivier@mnhn.fr

Electronic supplementary material is available online at https://doi.org/10.6084/m9.figshare.c.5046645.

Shells of the bivalve *Astarte moerchi* give new evidence of a strong pelagic-benthic coupling shift occurring since the late 1970s in the North Water polynya

Frédéric Olivier[1,12], Blandine Gaillard[2], Julien Thébault[3], Tarik Meziane[1], Réjean Tremblay[2], Dany Dumont[2], Simon Bélanger[4], Michel Gosselin[2], Aurélie Jolivet[3,13], Laurent Chauvaud[3], André L. Martel[5], Søren Rysgaard[6,7,8], Anne-Hélène Olivier[9], Julien Pettré[9], Jérôme Mars[10], Silvain Gerber[10] and Philippe Archambault[2,11]

[1]Laboratoire de 'Biologie des Organismes et Écosystèmes Aquatiques' (BOREA), Muséum national d'Histoire naturelle, Sorbonne Université, Université de Caen Normandie, Université des Antilles, Centre National de la Recherche Scientifique, Institut de Recherche pour le Développement-207, CP53, 61 rue Buffon, 75005 Paris, France
[2]Institut des sciences de la mer de Rimouski, Université du Québec à Rimouski, 310 Allée des Ursulines, Rimouski, Québec, Canada G5 L 3A1
[3]Institut Universitaire Européen de la Mer, Unité Mixte de Recherche 'Laboratoire des sciences de l'environnement marin' (LEMAR, UMR 6539), Centre National de la Recherche Scientifique, Institut de Recherche pour le Développement, Université de Bretagne Occidentale, Technopôle Brest-Iroise, rue Dumont d'Urville, 29280 Plouzané, France
[4]Département de biologie, chimie et géographie, Université du Québec à Rimouski, Québec-Océans et BORÉAS, 300 Allée des Ursulines, Rimouski, Québec, Canada G5L 3A1

THE ROYAL SOCIETY PUBLISHING

[5]Zoology Section (Malacology), Canadian Museum of Nature, PO Box 3443, Station D, Ottawa, Ontario, Canada K1P 6P4

[6]Greenland Climate Research Centre, Greenland Institute of Natural Resources, Kivioq 2, PO Box 570, 3900 Nuuk, Greenland

[7]Centre for Earth Observation Science, CHR Faculty of Environment Earth and Resources, University of Manitoba, 499 Wallace Building, Winnipeg, Canada MB R3T 2N2

[8]Arctic Research Centre, Aarhus University, C. F. Møllers Alle 8, 8000 Aarhus C, Denmark

[9]Université de Rennes, Inria, CNRS, IRISA, M2S, 35000 Rennes, France

[10]Grenoble Alpes, CNRS, Grenoble INP, GIPSA-Lab, 38000 Grenoble, France

[11]Arcticnet, Québec Océans, Takuvik, Département de biologie, Université Laval, 1045, avenue de la Médecine, Laval, Québec, Canada G1 V 0A6

[12]MNHN, Station Marine de Concarneau, place de la croix BP 225, 29182 Concarneau, France

[13]TBM Environnement/SOMME, 2 rue de Suède, Bloc 03, 56000 Auray, France

FO, 0000-0002-5776-8761; DD, 0000-0003-4107-1799; SR, 0000-0003-1726-2958

Climate changes in the Arctic may weaken the currently tight pelagic-benthic coupling. In response to decreasing sea ice cover, arctic marine systems are expected to shift from a 'sea-ice algae–benthos' to a 'phytoplankton-zooplankton' dominance. We used mollusc shells as bioarchives and fatty acid trophic markers to estimate the effects of the reduction of sea ice cover on the food exported to the seafloor. Bathyal bivalve *Astarte moerchi* living at 600 m depth in northern Baffin Bay reveals a clear shift in growth variations and Ba/Ca ratios since the late 1970s, which we relate to a change in food availability. Tissue fatty acid compositions show that this species feeds mainly on microalgae exported from the euphotic zone to the seabed. We, therefore, suggest that changes in pelagic-benthic coupling are likely due either to local changes in sea ice dynamics, mediated through bottom-up regulation exerted by sea ice on phytoplankton production, or to a mismatch between phytoplankton bloom and zooplankton grazing due to phenological change. Both possibilities allow a more regular and increased transfer of food to the seabed.

This article is part of the theme issue 'The changing Arctic Ocean: consequences for biological communities, biogeochemical processes and ecosystem functioning'.

1. Introduction

The Arctic region has been experiencing drastic environmental changes for the last few decades. Annual average near-surface air temperature has risen by 2–3°C since the 1950s [1,2] and the rate at which sea ice extent has declined is accelerating [3]. Polynyas are large areas of open water or reduced ice cover surrounded by thick pack ice. By remaining open in winter or becoming ice-free early in spring, polynyas are also local 'oases' for biological production and biodiversity that support large populations of arctic birds and mammals [4]. The ephemeral nature of polynyas makes them interesting regions for the study of large-scale processes related to climatic changes [5]. Some authors have suggested that monitoring the evolution of these sensitive areas will allow polynyas to serve as a model system for studying the impact of global changes on polar marine environments [5]. The North Water (NOW) polynya, also called Pikialasorsuaq, located in northern Baffin Bay, is the largest one in the Arctic ($5–8 \times 10^4$ km^2) which opens as early as April or May. The opening of this polynya is caused and maintained by persistent northerly winds and currents that carry ice away from an ice bridge between Greenland and Ellesmere Island [6,7], with secondary contributions of sensible heat from the West Greenland Current and upwelling in the east [8,9]. In order to assess the effects of climate change on Arctic marine

ecosystems, observations, data collection and monitoring over seasonal to decadal time scales are needed. Strictly speaking, characterizing climatic change requires past records of environmental conditions over several 30-year periods during which conditions can be assumed to be quasi-stationary. While such records exist for surface physical variables like sea ice, sediment, and temperature, this is more difficult for ecosystem indicators. In this context, biogenic archives provide a valuable assessment of the variability of marine ecosystems over the long term. Because of its longevity and low mobility, the benthos is reliable as an integrator of environmental conditions [10,11]. Seafloor communities can be used to examine impacts of environmental changes, since water column and benthic processes are often closely linked [12–16]. Furthermore, long-lived sessile benthic organisms are relevant monitors of variation in processes taking place in the overlying water column [13,17]. Bivalves often dominate the benthic biomass in the Arctic [18–20] and, as they incorporate information about ambient environmental conditions in their shells during biocalcification [21], such bioarchives contain both structural (growth; i.e. sclerochronology) and chemical proxies (stable isotopes, trace elements; i.e. sclerochemistry). Shells of most bivalves exhibit periodic banding, or growth lines [22,23] that have proved valuable in developing a history of environmental changes in marine systems [24–26]. The rate and timing of bivalve shell growth is controlled by regional and local environmental factors [27,28] such as temperature [22,24], age and reproductive cycle [29], tidal cycle [30], and nutrient and food availability [31], which can translate into a wide variety of annual and subannual (seasonal, lunar, fortnightly, daily and disturbance) growth patterns. For instance, long-lived (decades to centuries) bivalves have already been used to reconstruct past climate at the regional scale by relating their growth patterns with regional climate indices such as the North Atlantic Oscillation and the Arctic Ocean Oscillation, as well as local conditions such as ice cover and precipitation [32–36]. Coincident with periodic banding, growing shells incorporate minerals and chemicals that reflect specific environmental conditions at the time of shell formation. For instance, many studies have used stable oxygen isotope profiles from bivalve shells to reconstruct seasonal water temperature cycles, water masses, river discharge, and salinity [37–39]. Barium has also been used as a tracer for productivity and deep-water circulation [40]. Most bivalve Ba/Ca profiles seem to exhibit seasonal peaks in Ba which appear to be associated with changes in particulate and dissolved Ba or phytoplankton productivity [41–44].

In the present study, we focused on one bathyal population of the bivalve *Astarte moerchi*, one of the dominant taxa in terms of biomass in the community inhabiting the deep soft substratum of the NOW area [45]. We investigated the potential of *A. moerchi*, a long-lived (up to a century) [46] species, as a recorder of long-term environmental changes in the Arctic. Our main objectives were to (1) confirm that the formation of successive growth lines and increments in shells is annual, (2) investigate growth and Ba/Ca patterns, (3) explain growth and Ba/Ca regime shifts at a local scale with environmental (abiotic and/or biotic) parameters inherent to northern Baffin Bay and (4) confirm that fatty-acid (FA) trophic markers in tissues and the Ba/Ca ratio in shells are relevant tracers for monitoring primary production (PP) dynamics in bathyal arctic marine systems. We hypothesized that *A. moerchi* growth variability has tended to decrease during the last decades because the past tight sympagic-benthic coupling is expected to weaken in response to diminishing sea ice cover and the export of ice algae [47,48].

2. Methods

(a) Specimen collection

Fifty-one live *Astarte moerchi* were collected on 16 October 2010, from a depth of 568 m in northern Baffin Bay (Station 111; 76°11′ N; 73°12′ W; figure 1) using an Agassiz trawl deployed from the CCGS Amundsen. Individuals were sorted directly on the ship and then immediately frozen at −80°C. In the laboratory, all individuals were dissected on ice to separate soft tissues from shells. Tissues were stored at −80°C until lipid analysis, and shells were gently washed and air-dried until further analysis.

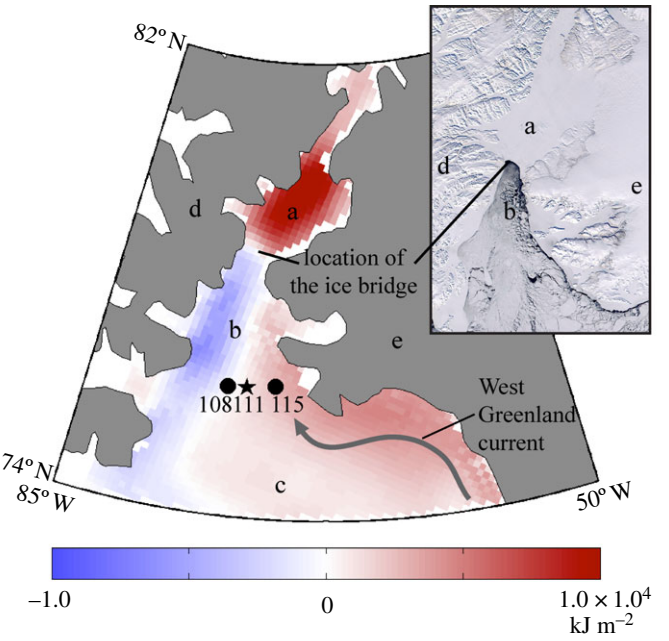

Figure 1. Location of stations 108, 111 and 115 in northern Baffin Bay. The map shows the difference between the average cumulated SWR at the sea surface, expressed in kJ m^{-2}, for years without the polynya (1990, 1993, 1995, 2007, 2009 and 2010) and the average climatological SWR (1979–2010). Blue and red colours represent either negative or positive anomalies. Northeastern Baffin Bay and Nares Strait upstream of the ice arch are regions of positive anomalies while western Smith Sound, along the Canadian coast downstream of the ice arch, shows a negative anomaly. Inset: A Moderate Resolution Imaging Spectroradiometer (MODIS) image of the open polynya on 23 April 2002. The ice bridge prevents sea ice from drifting in the polynya. (*a*) Kane Basin; (*b*) Smith Sound; (*c*) Baffin Bay; (*d*) Ellesmere Island, Canada; (*e*) Greenland. (Online version in colour.)

(b) Preparation of shell cross-sections

Shell cross-sections were made for growth and chemical (isotopic and elemental) analyses (see electronic supplementary material, S1 for a description of the analysed specimens). A low-speed precision saw (Secotom-10, Struers; rotation speed: 300 revolutions per minute; feed rate: 75 µm s^{-1}) with a 0.6 mm thick diamond-coated blade, cooled and kept wet using MilliQ water, was used to cut epoxy-embedded left valves along the line of maximum growth. These cross-sections were then mounted on glass slides, manually ground (800 and 1200 grit size), and polished with either Al_2O_3 powder (1 µm grain size) or a diamond suspension (1 µm grain size) for sclerochronological and sclerochemical analyses, respectively. Sections were then ultrasonically rinsed with MilliQ water to remove any adhering grinding powder. For sclerochronological analyses, sections were ground and polished down to an average thickness of 160 µm and images of the hinge sections of the shell were taken with a microscope at 40× magnification. For isotopic and elemental analyses, cross-sections were thicker (*ca* 800 µm and *ca* 750 µm, respectively). All samples were imaged and stitched (software AxioVision) using a stereomicroscope connected to a 5 megapixel camera at 80× magnification.

(c) Radiocarbon analysis

We performed radiocarbon analyses on six shells in order to establish whether or not the growth increments observed in shells of *A. moerchi* from northern Baffin Bay are annual. Aragonite samples were collected on four resin-embedded and two non-embedded right valves

to evaluate the potential risk of contamination of the radiocarbon signal by epoxy resin [49]. Three samples were collected from each shell (mass range: 1.3–4.3 mg) using a Merchantek computer-controlled MicroMill and a Dremel hand-held drill equipped with a 300 µm tungsten carbide drill bit. The first sample was taken close to the shell hinge, representing the older part of shell and presumed pre-bomb period; the second sample was taken from the central part of the shell presumably dating from the 1960s to 1970s and the abrupt increase of bomb radiocarbon signal; and the third sample was taken close to the ventral margin, from recent years of shell formation and the post-bomb period. The positions of samples were assessed from presumed annual growth lines counted on hinge cross-sections. Radiocarbon measurements were performed on graphite targets at the Centre for Accelerator Mass Spectrometry, Lawrence Livermore National Laboratory. Results included a background and $\delta^{13}C$ correction and are reported as $\Delta^{14}C \pm 1\sigma$ error [50]. We compared our results with three reference chronologies based on fish otoliths whose age was either known or could be estimated based on their length. The Northwest Atlantic (NWA) reference chronology is based on three fish species from the eastern coast of Canada and a bivalve from Georges Bank, Canada. The NWA chronology is a good proxy for the $\Delta^{14}C$ dissolved inorganic carbon history of the NWA. Radiocarbon data obtained from otoliths of the Greenland cod (*Gadus odac*) and Greenland halibut (*Reinhardtius hippoglossoides*) were used as radiocarbon reference chronologies for surface marine waters and deeper waters (300 m on average) of Davis Strait and western Greenland (see [51] for details).

(d) Growth pattern analyses

Increments in the hinge sections of nine shells were dated with the assumption that the last increment was produced in 2010 (sampling year). We evaluated observer bias by calculating the coefficient of variation (CV) between growth-line counts from six shell cross-sections by three distinct observers [52]. Increment widths were subsequently measured from images of the hinge section using the image analysis software ImageJ (Rasband 1997–2012, http://imagej.nih.gov/ij/). In order to identify changes in the shells' growth dynamics, we first calculated the difference in increment widths in the hinge sections for year n with respect to year $n-1$ for each shell (one individual). We then obtained a time-series of differences for each shell, named *diff_Variable* and applied the MATLAB function '*findchangepts* (diff_growth, 'Statistic', 'std')' on this time series to identify a change point in its standard deviation by minimizing a cost function over all possible locations of change points [53]. In addition, each time series was considered as a succession of periods whose number and dates of beginning and end (change points) have to be determined, and during which the annual growth of the shell is seen as constant with random noise ([54,55], as detailed in electronic supplementary material, S2*a–c*).

(e) Shell oxygen isotope analysis

Stable isotope oxygen analyses were performed on cross-sections of three *A. moerchi* shells. The oxygen isotope composition ($\delta^{18}O$) was measured on aragonite samples drilled in the outer shell layer of cross-sections using a Merchantek MicroMill equipped with a 300 µm tungsten carbide drill bit (model H71.104.003, Gebr. Brasseler GmbH & Co. KG). Due to spatial resolution limits set by the milling device and increment widths, each aragonite sample covered 1–3 years of shell growth. Between 42 and 55 samples were collected from each shell (mean mass = 112 µg). Samples were then analysed using a Finnigan MAT 253 continuous flow isotope ratio mass spectrometer (CF-IRMS) coupled to a GasBench II at the Institute of Geosciences of the University of Mainz, Germany. They were measured against an NBS-19 calibrated Carrara marble ($\delta^{18}O = -1.91‰$). Shell isotopic ratios are reported in conventional delta (δ) notation relative to the Vienna Pee Dee Belemnite (VPDB) standard [56]. Internal precision and accuracy were 0.07 and 0.04‰ VPDB, respectively.

(f) Laser ablation for Ba/Ca determination

The barium-to-calcium ratio was measured in the outer shell layer of three specimens (A73, A80 and A90). Analyses were performed using LA-ICP-MS, on a Thermo Element2 high-resolution inductively coupled plasma mass spectrometer (ICP-MS) coupled to a 193 nm laser ablation unit (COMPexPro 102, Coherent Inc.). Immediately before elemental analysis, shell cross-sections were pre-ablated in a fast-scanning mode to remove shell surface contamination (spot diameter of 80 µm and plate movement speed of 50 µm s^{-1}). The measurements were obtained by operating in a continuous sample mode (transects) at a translation speed of 5 µm s^{-1} (spot diameter of 80 µm), from ontogenetically young towards ontogenetically old shell portions. Signal intensities were recorded for ^{43}Ca and ^{138}Ba. ^{43}Ca was used as an internal standard to correct for variations in ablation yield caused by laser energy drift and sample density. Three standards were measured before each sample analysis to obtain a calibration to determine elemental concentrations. Absolute concentrations were converted to molar ratios (Ba/Ca), assuming 100% $CaCO_3$. Detection limits were estimated from the signal intensities of argon blanks (3σ) and were 0.16 µmol mol^{-1} for the Ba/Ca ratio.

(g) Fatty acid analysis

Total lipids of digestive glands of six specimens (see electronic supplementary material, S1 for details of specimens treated) were extracted using a solution of dichloromethane:methanol (2 : 1, v : v) following the Folch procedure [57]. Extracts were separated by column chromatography on silica gel micro-columns (30 × 5 mm inner diameter [i.d.] Kieselgel 70–230 mesh, Merck) using chloroform:methanol (98 : 2, v : v) to elute neutral lipids [58]. Neutral lipid fractions represent energetic lipids (mainly triacylglycerol) stored by the bivalves to support metabolism and growth. FA profiles were determined on FA methyl esters (FAMEs) using sulphuric acid : methanol (2 : 98, v : v) and toluene. FAMEs of neutral lipids were concentrated in hexane and analysed in mass spectrometry scan mode (ionic range: 50–650 *m/z*) on a Polaris Q ion trap coupled to a Trace GC Ultra multichannel gas chromatograph (Thermo Scientific) equipped with a Triplus autosampler, a PTV injector and a mass detector, model ITQ900 (Thermo Scientific). The separation was performed with an Omegawax 250 (30 m × 0.25 mm i.d.) capillary column with high-purity helium as a carrier gas. FAMEs were identified by comparing retention times with known standards (Supelco 37 Component FAME Mix and menhaden oil; Supelco Inc., Belfonte, PA, USA), using Xcalibur v. 1.3 software (Thermo Scientific). The mass of total FA was expressed as mg g^{-1} of tissue dry mass, and FA composition was expressed as the relative proportion of each fatty acid.

(h) Physical data and remote sensing

Surface air temperatures were obtained from the National Centre for Environmental Prediction Re-analysis. Cumulative short-wave radiation (SWR) was calculated using total cloud-cover data from the European Centre for Medium-Range Weather Forecasting ERA-Interim Re-analysis over two regions assimilated as boxes of approximately 12 000 km^2, centred in either Kane Basin (79.5° N, 70.4° W) or Smith Sound (77.6° N, 73.1° W). Sea ice concentration was determined from the MyOcean Ocean and Sea Ice Satellite Application Facility. Ice charts from the Canadian Ice Service and from the Danmarks Meteorologiske Institute were used to assess the break-up date of the ice bridge and its variability over a 45-year period (1968–2010).

Monthly maps of PP were calculated from satellite observations of ocean colour, sea ice, and cloud cover based on the approach developed in Bélanger *et al.* [59] (detailed in electronic supplementary material, S3). The performance of this satellite-based PP model, developed specifically for the Arctic Ocean where optically complex waters and sea ice are present, was better than most PP models currently available (among more than 30 models) [60].

(i) Phytoplankton production and taxonomic composition

During the autumns of 1999 and 2005 to 2010, particulate PP rates were measured at 7 depths within the euphotic zone (corresponding to 100, 50, 30, 15, 5, 1 and 0.2% of surface photosynthetically active radiation using the ^{14}C-uptake method [61,62] at stations 108 and 115; figure 1). Samples containing ^{14}C were incubated for 24 h under simulated *in situ* conditions in a deck incubator with running surface seawater. PP rates were integrated for euphotic zone depths using trapezoidal integration. Production rates of small (0.7–5 µm) and large ($\geq$ 5 µm) phytoplankton cells were considered. Detailed information about PP measurements can be found in [63,64]. In the autumns of 2005–2010, phytoplankton were also sampled from surface waters and at the depth of the subsurface maximum fluorescence and preserved in acidic Lugol's solution [65]. Cells (greater than 2 µm) were identified to the lowest possible taxonomic level using the inverted microscope method [66].

(j) Statistical analysis

Statistical analyses were carried out with the free software R, v. 3.5.0. We used locally weighted least square (LOESS) regressions (span = 0.45) to visualize bomb radiocarbon patterns over time. Coefficients of variation (CV) were calculated to assess both inter-reader variability of age determination of shells and inter-shell variability for oxygen isotope data: CV is the standard deviation of one variable divided by its mean and expressed in %. A Mann–Whitney test (for data not normally distributed) was then used to compare mean δ^{18}O values between the three shells. We also compared mean Ba/Ca values assessed for either 1977–2010 or 1927–1976 by using a Wilcoxon signed-rank test (homoscedasticity not satisfied). Simple linear regressions were performed on average annual temperature and SWR datasets and included in the related figures. Variations in phytoplankton community structure among years were evaluated using a distance-based permutational multivariate analysis of variance (PERMANOVA) based on Bray–Curtis dissimilarities and visualized using non-metric multidimensional scaling (nMDS) ordination using PRIMER 6 [67,68].

3. Results

(a) Radiocarbon

Δ^{14}C values from resin-embedded and non-embedded samples were similar during pre-bomb and post-bomb periods. We can, therefore, conclude that any effect of resin contamination on Δ^{14}C values was negligible. Δ^{14}C values ranged between -82.02 ± 5.33 and 8.34 ± 4.80‰ (figure 2). Despite its smaller amplitude, the Δ^{14}C pattern in the shells of *A. moerchi* was similar to bomb radiocarbon reference chronologies, with relatively low and stable pre-bomb values (prior to 1957, in theory) followed by increasing values after 1960. Pre-bomb values in shells of *A. moerchi* were virtually identical at a Δ^{14}C of about –70‰ in the NWA and Arctic deep-water (Greenland halibut otoliths) chronologies. Δ^{14}C levels after 1960 were clearly distinct between shells of *A. moerchi* and reference chronologies. The highest Δ^{14}C values were reached later (after 2000) than in the NWA and Arctic water reference chronologies (between the 1960s and 1980s).

(b) Growth pattern

Astarte moerchi specimens used for sclerochronological analyses ($N = 9$) were aged between 61 and 109 years old. Diagrams of mean increment width in either the hinge tooth or in the outer shell layer versus age are shown in figure 3. Based on the shells, we estimated that the inter-reader variability (CV) between counts was 8.0% in the hinge region and 4.2% in the external layer. Single and multiple individual CPY growth analyses are detailed in electronic supplementary material, S2a,c. Single change-point (CP) detection analyses revealed that the increment dynamics of five

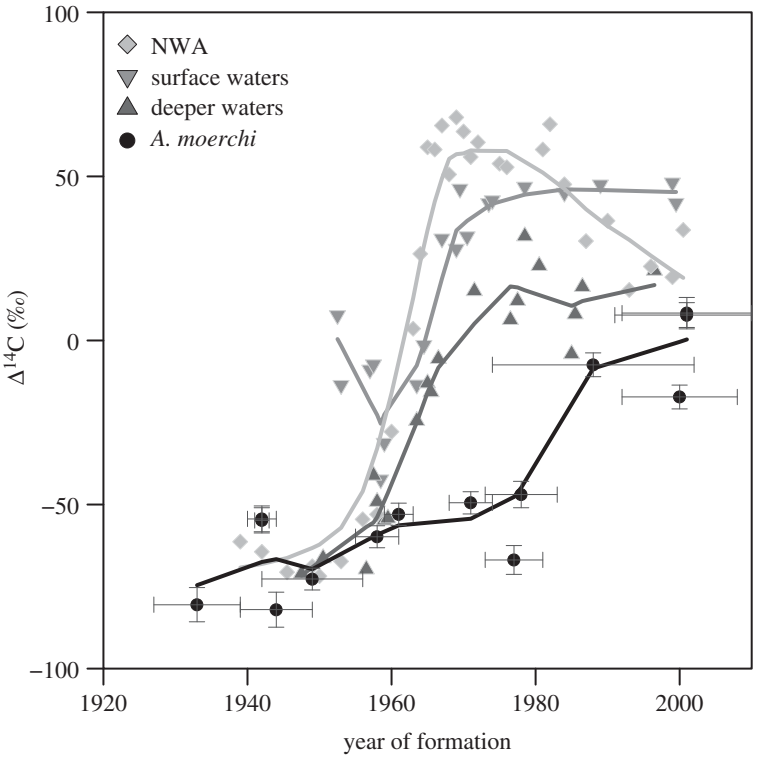

Figure 2. Bomb radiocarbon chronologies for *Astarte moerchi* (black circles). Horizontal bars are estimated sampled period for $\Delta^{14}C$ analysis. Fitted lines are locally weighted least square (LOESS) regressions. Reference chronologies are from Campana *et al.* [49]: marine Northwest Atlantic (NWA) reference chronology (light grey diamond), arctic marine surface waters (0–100 m) (grey downward triangle), and arctic marine deep waters (300 m on average) (dark grey upward triangle).

or six shells followed two different regimes, separated by a change point year (CPY) between 1971 and 1987 (mean CPY = 1981.6 ± 1.7 s.e. or 1977.3 ± 2.7 s.e., from the Trauth [53] or Lavielle & Moulines [54] methods, respectively, table 1). However, that was not the case for the other three or four shells which displayed either earlier (1953.0 ± 2.0 s.e. or 1952.6 ± 1.3 s.e., respectively) or later (2004.5 ± 3.5 s.e., table 1) CPY. Multiple CP detection analyses revealed three main periods of shifting regime (figure 4*a*) around the late 1930s (mean CPY = 1938.0 ± 1.4 s.e., $N = 8$), 1950s (mean CPY = 1953.0 ± 1.8 s.e., $N = 6$), and the late 1970s (mean CPY = 1977.1 ± 2.8 s.e., $N = 7$). Overall bivalve growth was, in fact, more variable before the late 1970s (13.4 < standard deviation σ < 18.7 µm, mean σ = 15.1 µm) than during the last three decades (3.9 < σ < 7.3 µm, mean σ = 5.4 µm).

(c) Shell oxygen stable isotopes

No ontogenetic trends were observed for oxygen stable isotopes. The $\delta^{18}O$ profiles displayed low variability for each of the three shells (CV < 9.4%) and among them (mean CV = 5.28%, $n = 3$) (figure 5). Although the mean $\delta^{18}O$ value from shell A98 (5.06 ± 0.27‰) was significantly greater than that of shells A41 and A76 (4.95 ± 0.26‰ and 4.84 ± 0.46‰, respectively, $p < 0.05$), the values remained stable for a 50-year period.

(d) Ba/Ca ratios

By contrast, time series of mean annual Ba/Ca ratios for the three specimens, ranging from 1.33 to 50.08 µmol mol^{-1}, showed relatively similar patterns with a flat background level

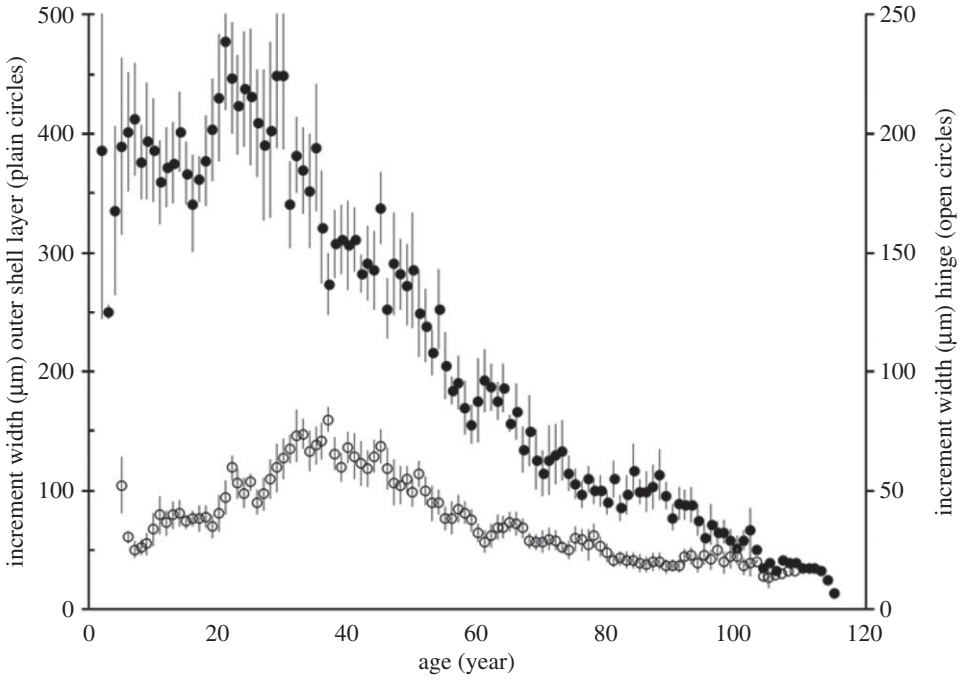

Figure 3. Mean increment width (± s.e.) at age in the hinge (open symbol) and the outer shell layer (black symbol) of *Astarte moerchi*.

Table 1. Results of the change points years (CPY) detection analyses performed on the increment width time series of nine *A. moerchi* shells and on Ba/Ca mean annual ratios of three *A. moerchi* shells. CPY analyses were with either single or multiple (up to three) changepoints (see methods for details, either from Trauth [53] or Lavielle and Moulines [54] and Lavielle [55]). Years around 1970–1980s corresponding to the most abundant group are given in italics.

Ind.	Nb. of increments	CPY (single) [53]	CPY (single) [55]	CPY (multiple) [55]	CPY (multiple) Ba/Ca [55]
A39	103	1955	1954	1941, 1954	
A41	97	2001	*1987*	1941, 1957, *1987*	
A50	80	1951	1950	1939, 1950	
A59	76	*1987*	1954	1942, 1949, *1967*	
A73	101	*1983*	*1984*	1932, 1943, *1987*	*1979*, 1999, 2004
A76	86	2008	*1971*	1934, 1959, *1977*	
A80	94	*1979*	*1973*	1937, 1949, *1973*	*1977*, *1979*
A90	82	*1977*	*1975*	*1975*	*1975*, 2000
A94	79	*1982*	*1974*	*1974*	

interrupted by several sharp peaks. Mean annual Ba/Ca ratio based on the three shells ranged from 2.85 to 19.88 µmol mol^{-1}, and the frequency and intensity of their peaks tended to increase after 1977 (mean CPY = 1977.0 ± 1.2 SE, table 1), the mean value calculated for the last 34 years (9.21 ± 0.52 µmol mol^{-1}, 1977–2010) being twice that of the previous 50 years (4.23 ± 0.12 µmol mol^{-1}, 1927–1976) ($p < 0.001$) (figure 4*b*). Interestingly, CP analyses also detected one additional more recent CPY in 2002.0 ± 2.0 SE for two of the three shells (see electronic supplementary material, S2b for individual graphs).

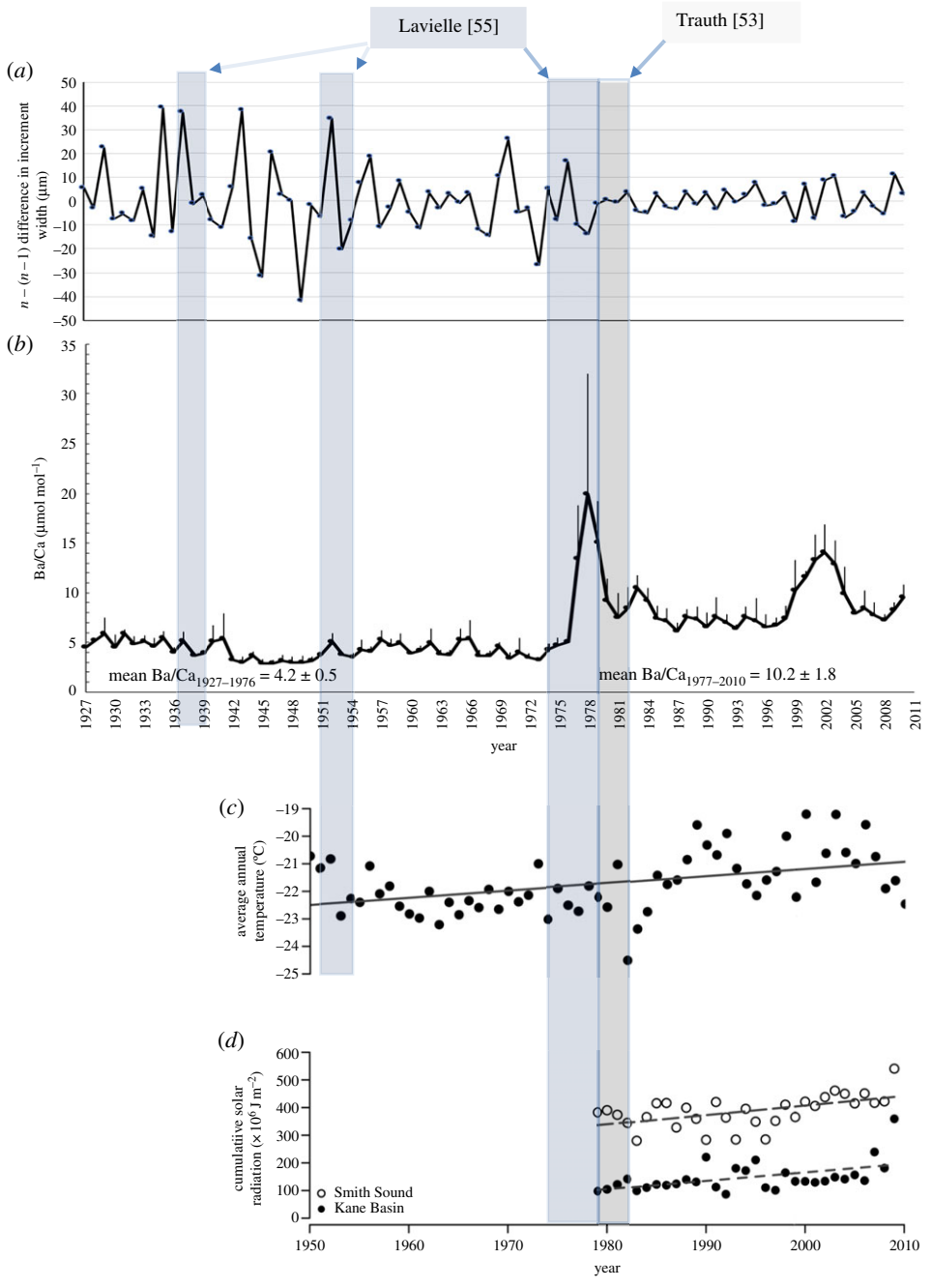

Figure 4. Time series of (*a*) standard deviation of the difference in increment width during year *n* minus year *n* − 1 of one *Astarte moerchi* shell (A80), (*b*) mean annual Ba/Ca ratios measured on cross-sections of three *A. moerchi* shells from northern Baffin Bay (A73, A80 and A90, Sta. 111), (*c*) average annual temperature and (*d*) cumulative SWR at the sea surface in Smith Sound and Kane Basin with simple linear regressions of $y = 3.461x - 6514$ ($R^2 = 0.293$) or $y = 3.082x - 5998$ ($R^2 = 0.272$), respectively. Grey/White bars indicate mean change points year ± s.d. of either Lavielle [53] or Trauth [51] analyses.

(e) Fatty-acid profiles

The main food sources of *A. moerchi* were determined using the FA composition of neutral lipids of the digestive gland of these filter feeders. The detailed FA compositions are presented in table 2.

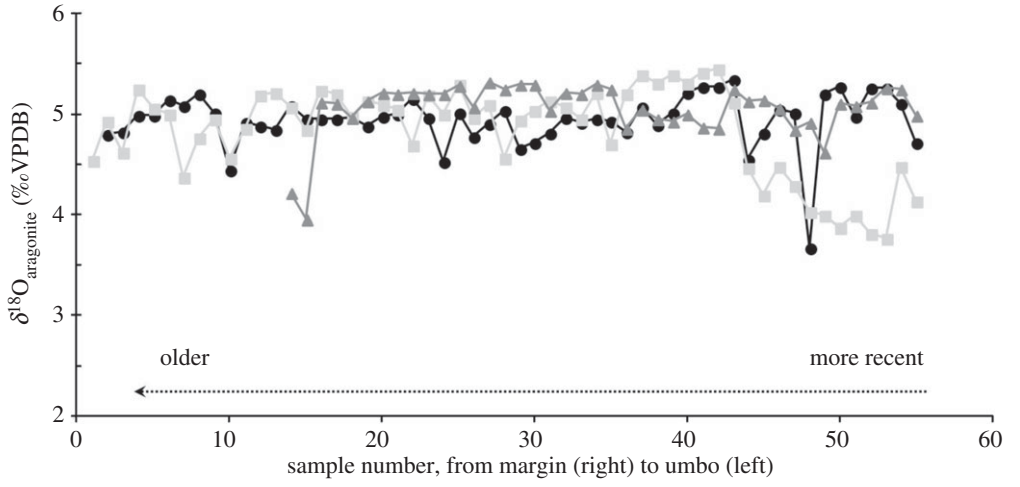

Figure 5. Stable isotope oxygen profiles from cross-sections of the three *Astarte moerchi* shells (same as those of Ba/Ca profiles) from northern Baffin Bay (Sta. 111).

Saturated fatty acids (SFA) were dominated by 16 : 0 and 18 : 0. Branched fatty acids proportions were very low (less than 1%), monounsaturated fatty acids (MUFA) were dominated by 16 : 1ω7, 20 : 1ω7 and 18 : 1ω7, and the pool of polyunsaturated acids (PUFA) mainly comprised 20 : 5ω3 eicosapentaenoic acid (EPA), 22 : 6ω3 docosahexaenoic acid (DHA) and 20 : 4ω6 arachidonic acid (AA).

(f) Physical environment and primary production dynamics

Figure 4*c* shows a 62-year time series of annual mean surface air temperature in Kane Basin. This period is characterized by a slight warming trend, which becomes more obvious over the last three decades. The same trend is observed for the cumulative SWR (in J m^{-2}) at the sea surface with increases of 23% in Smith Sound and 38% in Kane Basin between the periods 1979–1990 and 2000–2010 (figure 4*d*). Data were not available for this region before the late 1970s, and therefore we were able to focus on the evolution of the physical environment and PP dynamics over only the last three decades.

The cumulative SWR reaching the ocean surface below the ice over the spring–summer period is used here as a proxy to highlight potential changes in PP pattern in space. The differences at various sites between the cumulative SWR averaged over all years during which a polynya did not form (1990, 1993, 1995, 2007, 2009 and 2010) and that averaged over all years when it formed over the 1979–2013 period is presented in figure 1. There were significant increases in western Smith Sound, Baffin Bay, and to a greater extent in Kane Basin, while there was a reduction in eastern Smith Sound, along the Canadian coast, consistent with reduced ice cover extent and duration, but also with the disruption of the ice bridge. When the ice bridge does not form, ice flows southward along the Canadian coast and thus reduces the SWR over that area, while increasing it in the region upstream.

Monthly summer (May, June and July) PP trends in northern Baffin Bay and Smith Sound from 1998 to 2010 computed for each SeaWiFS 9.28 × 9.28 km pixel are shown in figure 6. Positive values (in red) indicate increasing trends in the monthly PP, which was the case in May, with increasing trends reaching approximately 1 g C m^{-2} $month^{-1}$ $year^{-1}$ between 1998 and 2010. In June and July, by contrast, we observed strongly negative trends (in blue) suggesting that the monthly PP has declined at rates as great as 2 g C m^{-2} $month^{-1}$ $year^{-1}$ during the period considered. This negative trend, estimated from satellite-based methods, was also confirmed by *in situ* observations. PP measured during the autumns of 1999, 2005–2008 and 2010 decreased on the Greenland side

Table 2. Relative fatty acid (FA) composition of the neutral fraction of *Astarte moerchi*'s digestive gland. Fatty acid values are mean % of the mass of total fatty acids ± standard error (s.e.). Only FA greater than 1% are shown, excluding branched FA. Important trophic markers are highlighted in bold: branched fatty acids are bacterial markers, 16 : 1ω7 and 20 : 5ω3 are the markers for diatoms, 18 : 4ω3 and 22 : 6ω3 are markers of dinoflagellates, and 20 : 1ω9 is marker of zooplankton. *i*-: iso- fatty acid; *ai*-: anteiso- fatty acid; SFA, saturated fatty acids; MUFA, monounsaturated fatty acids; PUFA, polyunsaturated fatty acids; AA, arachidonic acid; EPA, eicosapentaenoic acid; DHA, docosahexaenoic acid; MTFA, mass of total fatty acids.

fatty acid	relative proportion (mass % ± s.e.)
***i*-15 : 0**	0.07 ± 0.03
***i*-16 : 0**	0.79 ± 0.21
16 : 0	11.75 ± 0.49
***i*-17 : 0**	0.82 ± 0.08
***ai*-17 : 0**	0.44 ± 0.06
***i*-18 : 0**	0.26 ± 0.12
18 : 0	3.78 ± 1.21
Σ SFA	20.15 ± 2.21
16 : 1ω7	17.26 ± 3.34
18 : 1ω9	2.04 ± 0.21
18 : 1ω7	4.51 ± 0.43
18 : 1ω5	4.11 ± 0.43
20 : 1ω11	2.43 ± 0.28
20 : 1ω9	1.11 ± 0.19
20 : 1ω7	7.60 ± 1.24
20 : 1ω5	3.00 ± 0.29
Σ MUFA	44.22 ± 1.76
16 : 2ω4	2.13 ± 1.42
18 : 4ω3	1.87 ± 0.33
18 : 2ω6	0.88 ± 0.11
20 : 4ω6 (AA)	2.35 ± 0.89
20 : 5ω3 (EPA)	17.77 ± 1.83
22 : 5ω3	1.01 ± 0.23
22 : 6ω3 (DHA)	4.90 ± 0.18
Σ PUFA	35.63 ± 1.54
ratios	
16 : 1ω7/16 : 0	1.52 ± 0.30
$\Sigma C_{16}/\Sigma C_{18}$	1.86 ± 0.27
EPA/DHA	3.68 ± 0.41
MTFA mg g^{-1}	7.80 ± 3.50

of northern Baffin Bay. At station 108, PP decreased from 2.36 g C m^{-2} d^{-1} in 1999 to 0.05 g C m^{-2} d^{-1} in 2010, whereas the decrease was less pronounced at station 115, decreasing from 0.72 g C m^{-2} d^{-1} to 0.04 g C m^{-2} d^{-1} between 1999 and 2010 (figure 7*a*,*b*). Moreover, this trend

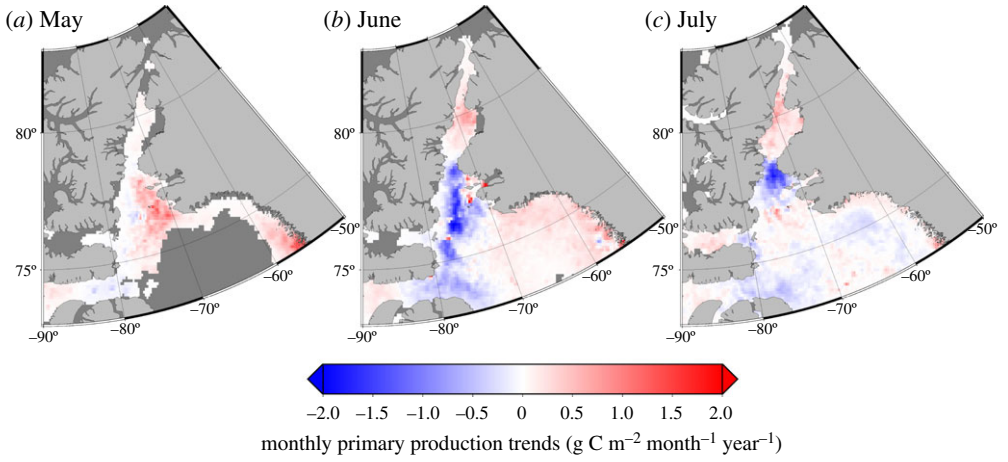

Figure 6. Trends in monthly primary production (in g C m^{-2} $month^{-1}$ $year^{-1}$) in northern Baffin Bay and Smith Sound from 1998 to 2010 as assessed by remote sensing following Bélanger *et al.* [59] with SeaWiFS monthly data. (Online version in colour.)

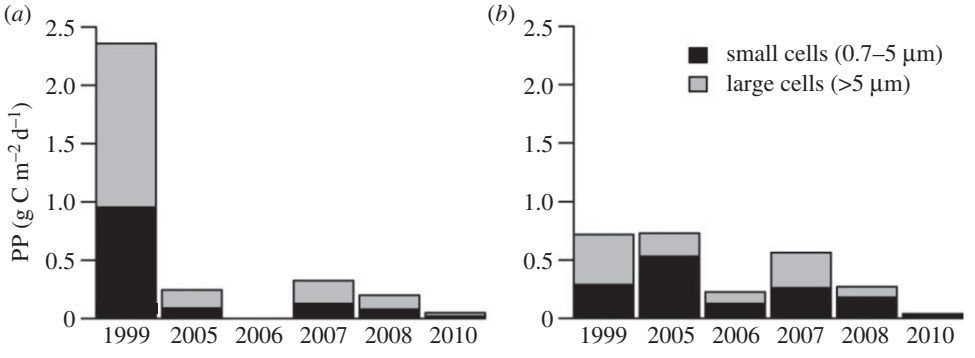

Figure 7. Variations in primary production (PP) for small (0.7–5 µm) and large (greater than 5 µm) cells integrated over the euphotic zone at Sta. (*a*) 108 and (*b*) 115 during autumn. Data of 1999 are from Klein *et al.* [63].

was associated with a decrease in the contribution of large (greater than 5 µm) and small (0.7–5 µm) cells to total phytoplankton production (figure 7). However, since 2005, the structure of phytoplanktonic assemblages has been highly variable. Figure 8 shows that there was no clear evolution of phytoplankton assemblages from 2005 to 2010 (e.g. from a majority of diatoms to more flagellates).

4. Discussion

Shell growth rate is largely governed by temperature and food availability [69]. It is generally assumed that high-latitude species deposit darker growth lines in winter [70] when low temperatures and a lack of food cause individuals to stop growing or grow very slowly. In the present study, we used bomb radiocarbon dating as evidence that growth-line deposition in the shells of *A. moerchi* is annual. We observed delayed and reduced amplitude of $\Delta^{14}C$ values compared with reference chronologies. However, since shells were collected in approximately 600 m depth water, this may result from the transit time of the bomb signal from surface to deeper waters and the reservoir effect [71]. $\Delta^{14}C$ values showed that formation of more than one growth line every year is impossible, since the more ^{14}C-depleted data related to pre-bomb signal would

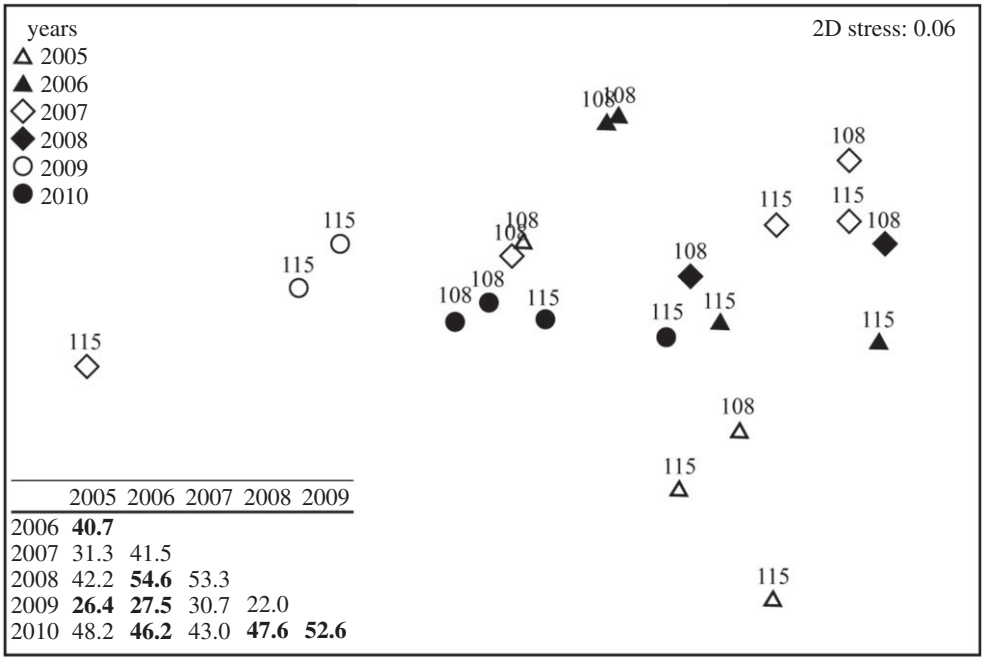

	2005	2006	2007	2008	2009
2006	**40.7**				
2007	31.3	41.5			
2008	42.2	**54.6**	53.3		
2009	**26.4**	**27.5**	30.7	22.0	
2010	48.2	**46.2**	43.0	**47.6**	**52.6**

Figure 8. Non-metric multidimensional scaling (nMDS) ordination based on the Bray-Curtis dissimilarity matrix calculated on untransformed protist group (greater than 2 µm) abundances. Samples were collected at Sta. 108 and 115 between 2005 and 2010. Before performing the nMDS, the taxa were grouped into six categories: (1) C-diatoms (*Chaetoceros* spp.), (2) T-diatoms (chain-forming centric diatoms), (3) M-diatoms (filament-forming diatoms), (4) dinoflagellates, (5) flagellates and (6) ciliates, including Tintinids. The table indicates the average percentage similarity between years. Years that differ significantly ($p < 0.05$) are highlighted in bold.

be after the 1970s. On the other hand, one growth line every 2 years is very unlikely in view of stable abiotic conditions (temperature, salinity, etc.) in the surrounding deep environment habitat of *A. moerchi*. To our knowledge, only PP dynamics exhibiting an annual rhythmicity resulting in a strong seasonal variation of food availability in Arctic systems may lead *A. moerchi* to produce clearly separated growth increments. Hence, radiocarbon analysis confirmed that the formation of growth lines in shells of *A. moerchi* is annual.

The oxygen isotopic composition ($^{18}O/^{16}O$) of marine carbonate is controlled by the temperature and isotopic composition of the ambient water ($\delta^{18}O_{water}$) from which it precipitated. Because the $\delta^{18}O_{water}$ is primarily influenced by salinity and thus by freshwater inputs [72], establishing oxygen isotopic profiles along the axis of maximum growth of the carbonate shells allows one to extract hydrographic time-series information on the bivalve's habitat. Low ontogenetic variation in the oxygen isotope composition of *A. moerchi* shells demonstrates that water temperature and salinity were both very stable throughout the bivalve's lifetime, which is expected at an ocean depth of 600 m. Therefore, we hypothesize that food supply is the main environmental factor explaining the shift in the growth patterns of *A. moerchi*.

Some FA, because they are mainly or exclusively synthesized by particular algal classes in an aquatic environment [73], can thus be used as biomarkers in organic matters or consumer tissues. For instance, diatoms are characterized by high proportions of 16 : 1ω7, C_{16} PUFA, and 20 : 5ω3, while flagellates and dinoflagellates are characterized by elevated C_{18} PUFA (particularly 18 : 4ω3) and C_{22} PUFA (especially 22 : 6ω3) [73,74]. The FA composition of neutral lipids from digestive gland tissue suggests that the major constituents of *A. moerchi*'s diet are microalgae (mainly diatoms) exported from the euphotic zone to the seabed. Similarly, in a previous study [75], coastal populations of *A. moerchi* from the Young Sound fjord exhibited high contributions of

20 : 5ω3 (EPA) and 16 : 1ω7, as well as a ratio of 16 : 1ω7/16 : 0 of greater than 1.5 in their digestive glands, as also observed here, strongly suggesting that diatoms make up an important part of their diet, supporting the results of this study. Similar observations were made on the bivalve *Bathyarca glacialis* across the Canadian Arctic archipelago [76]. Indeed, despite *B. glacialis* from the northern Baffin Bay and Lancaster Sound living at a depth close to 800 m, the presence of typical PUFA markers in their tissues suggested that they benefit from microalgae exported from the euphotic zone.

Furthermore, Ba/Ca ratios, used in coastal areas as a proxy for the timing and magnitude of diatom blooms for the tropical filter-feeding scallop *Comptopallium radula* [44], support the hypothesis of a succession of blooms during the whole life of the bivalve. For the other long-lived species *Arctica islandica*, the synchrony of Ba/Ca time series between living specimens of one single population/site is now well accepted, and higher annual mean Ba/Ca shell ratios can be related to primary productivity [43]. The frequency and intensity of mean annual Ba/Ca peaks from *A. moerchi* shells clearly increased beginning in the late 1970s. Interestingly, the same regime transition was also obvious from the shells' growth data, in five to six (depending on the model used in change point analyses) of the nine shells analysed.

In terms of detrital or bacterial contributions to *A. moerchi* diet, their relative markers were weakly detected (ratio $[16:0+18:0]/\sum\text{PUFA} < 0.5$, and 2.4% of total branched FA, respectively) confirming that this bathyal system's filter-feeder bivalve mainly assimilated recent fresh organic matter.

The present work suggests that, over the last half-century, the pelagic-benthic coupling in northern Baffin Bay may have intensified through a more regular export of food supply of diatom origin from the euphotic zone to the bottom. This completes and adds nuance to the current hypothesis arguing that climate change will benefit the pelagic food chain (phytoplankton–zooplankton), but be detrimental to the zoobenthos [77,78]. We propose the following two hypotheses to explain this temporal pattern.

(a) Local physical conditions

If changes in the growth regime of filter-feeding bivalves at 600 m depth are related to climate change, they should ensue from variations in the local dynamics of primary producers. The growth pattern of *A. moerchi* is thus possibly related to large-scale environmental patterns affecting sea ice, with the main drivers acting at a regional or local scale. In the case under investigation, the presence of a recurrent polynya constitutes a strong driver that deserves closer evaluation.

The NOW polynya forms when persistent northerly winds push ice away from the landfast ice covering Kane Basin. The southern limit of this landfast ice cover is often referred to as an ice bridge. This bridge plays a central role in the formation of the polynya as without it, sea ice flows continuously following winds and currents and the polynya simply does not exist as a persistent and localized feature. The position and shape of the ice bridge are very stable, but the time of formation and break-up are highly variable from one year to another [79]. This means that the ice bridge controls the timing and the area over which light will or will not penetrate the ocean. Since landfast ice is immobile by definition, the ice thickness and strength are mostly controlled by thermodynamics, which are determined to a large extent by the local surface air temperature. During a cold winter, the ice is likely to become thicker, be resistant to stronger forces, and survive longer during the melt season. The relation between surface air temperature, which tends to increase, and ice distribution in the area is not linear but depends, for instance, upon the highly nonlinear and heterogeneous dynamic ice behaviour. Two kinds of changes are nonetheless expected, in the timing and in the quantity of ice over the spring–summer period, both of which affect the spatio-temporal distribution of light penetration into the ocean. Based on ice charts produced by the Canadian Ice Service over the last five decades, we conclude that the ice bridge broke up on average two weeks earlier during the 1994–2012 period compared with the 1968–1993 period. In addition, the frequency of occurrence of the

NOW polynya decreased from almost 100% (1968–1993) down to 70% (2002–2012). When the ice bridge does not form, sea ice flows uninterruptedly through the channel so that the concentration of ice in Kane Basin drops while that of Smith Sound increases slightly, compared with the climatology. Changes in the spatio-temporal distribution of sea ice have significant effects on light availability. This is quantified by integrating the incident SWR that effectively reaches the ocean surface, that is, after being attenuated by clouds and sea ice over the year. This is shown in figure 1 in the cumulative SWR anomaly between polynya versus no-polynya years. In fact, higher cumulative SWR should lead to a general increase in PP in the Arctic Ocean and its marginal seas [80] where enough nutrients are available in the euphotic zone [64,81]. As a result of the controlling effect of sea ice on phytoplankton production and, hence, food availability for the bivalves, correlations between local sea-ice cover and the growth rate of benthic organisms can be expected and have already been observed. Very high concentrations of sea ice can be viewed as an inhibitor of PP and the growth of consumers, and, by contrast, a low sea-ice cover leads to increased PP and food availability for the benthos. For example, sea urchin (*Strongylocentrotus droebachiensis*) growth performance is limited by food, especially in high-Arctic areas where sea-ice cover influences annual primary productivity [82]. This trend is supported by a study [36] that showed a correlation between an annual index of ice cover and the growth rate of the Arctic cockle *Clinocardium ciliatum*. It is, therefore, plausible that the growth performance of bivalves in Baffin Bay was regulated from the bottom up through the impact of sea ice on phytoplankton production, which we now explore.

(b) Spatio-temporal mismatch hypothesis

Despite observations that Arctic marine ecosystems are becoming more productive in several areas and the expectation that this increase should promote pelagic food webs (phytoplankton–zooplankton) [48], the results presented here and in previous studies imply that global environmental changes can drive contrasting responses at smaller spatial scales, with unknown local effects on benthic productivity.

Remote-sensing investigations of northern Baffin Bay and Smith Sound have shown that phytoplankton phenology has changed, with spring bloom onset occurring earlier and with a weaker intensity [83]. A concomitant decline in satellite-based estimates of PP has been reported for the period 1998–2010 [59] and confirmed by *in situ* data showing a decrease in seasonal nitrate consumption by phytoplankton [84] and a decline in daily PP rates in late summer and fall [79]. These negative trends can be partly attributed to enhanced vertical stratification in the NOW [84] and a northward shift of the high productivity zone toward Kane Basin [85], where local phytoplankton growth presumably reduces horizontal nutrient supply into Smith Sound. Such recent changes in the phenology and magnitude of PP lead us to suggest that a greater match between pelagic food production and the benthic filter feeders is now occurring.

Despite uncertainties about horizontal ocean currents from the surface to the bottom and the vertical sinking velocity profiles of phytoplankton cells, it can be presumed that a horizontal shift in the food source could change its location of arrival at the bottom. As an example, Johnsen *et al.* [86] revealed that an under-ice bloom observed in May 2010 at Northwest Svalbard originated in fact from the advection of an open water bloom that occurred at the south of the ice edge. Furthermore, reductions in the horizontal and vertical supplies of nutrients to the upper euphotic zone in the NOW are conducive to an increase in the relative contribution of subsurface phytoplankton communities to annual PP. These communities, which have been known to be present and active in the NOW, exploit elevated nutrient concentrations at the base of the euphotic zone and are generally dominated by shade-adapted diatoms of the genus *Chaetoceros*, particularly *C. gelidus* (formerly *socialis*) [87,88]. This scenario is consistent with an upward numerical shift of *Chaetoceros* spores between 1968–1993 and 1994–2012 in one sediment core from Smith Sound (collected in 2015 at 692-m depth, *ca* 66 miles north of station 111; A.L. Limoges, personal communication, 2020). A global review of the seasonally persistent diatoms that compose shade flora in subsurface layers has shown that they are typically exported later in

the productive season (sometimes in early fall), contrasting with other diatom genera that sink early with the spring bloom [89]. Diatoms are the primary food source of *A. moerchi* and the evidence provided here strongly suggests that the quality and timing of food deliveries to the benthos has changed in the NOW.

Changes in the phytoplankton communities in northern Baffin Bay [79] could alter both the quality and quantity of the food supply exported to higher trophic levels, especially within the benthic environment. The high variability of phytoplankton assemblages since 2005 suggests changes in PP quality from year to year without any influence on the growth pattern observed in *A. moerchi* shells. While a decline in the quantity of food supplied to the benthos was expected (because of the decline of the PP in surface waters), the observed growth variations and Ba/Ca temporal dynamics in bivalve shells, shifting drastically around 1978, lead us to hypothesize that a larger abundance/biomass of diatoms reaches the seabed. One possible mechanism to account for this is a mismatch [90] between phytoplankton and zooplankton dynamics. Grazing by herbivorous zooplankton largely determines the contribution of primary producers to benthic systems. Recent Arctic studies that focus on links between primary and secondary producers in a changing sea-ice cover suggest a potential mismatch between the phytoplankton bloom and the temperature-controlled ontogenetic development of zooplankton (mainly *Calanus glacialis*) [91,92]. Boetius *et al.* [93] advanced the hypothesis that the current sea-ice thinning may enhance under-ice productivity and ice-algae export. However, years with less ice coverage, caused by earlier ice break-up, reduced ice and snow cover, or both, will thus lead to a shorter temporal time lag between the ice algal and phytoplanktonic blooms, resulting in a potential mismatch [91]. Timing is the single most essential factor controlling the recruitment and development success or failure of pelagic secondary producers [90]. Timing will, therefore, determine how efficient the biomass and energy transfer to higher pelagic trophic levels or how much greater export to the bathyal benthic communities will be. Our study shows a positive PP trend in May, followed by a decreasing trend in June–July, suggesting that the phytoplankton bloom now occurs earlier in the season than it did previously in northern Baffin Bay. More importantly, despite such significant evolution in the surface waters of the NOW polynya, no regime shift in the growth dynamics of *A. moerchi* could be detected between 1998 and 2010. The timing of phytoplankton bloom in northern Baffin Bay may have shifted to earlier in the season, and its intensity may have weakened, resulting in lower annual PP [59,83]. In addition, shifts to earlier phytoplankton blooms have been observed in other locations across the subarctic seas [94]. Unfortunately, the lack of older data before the late 1970s makes it difficult to draw conclusions about the real origins of the bivalve growth regime shift. Moreover, it is difficult to explain the contrasting growth pattern of the two other shell groups displaying either older (1950s) or earlier (2000s) tipping points (single CPY methods) as well as older CPY (1940s and 1950s, multiple CPY methods). Small-scale heterogeneity of food export to the seabed, as well as the influence of the reproduction cycle of such long-lived species for which no data are currently available, have to be mentioned as potential sources of inter-individual variability.

In conclusion, the marine bivalve *A. moerchi* shows unexpectedly less-variable growth since the late 1970s, a fact that may be explained by a greater and more regular export of food to the seafloor, resulting either from a temporal mismatch between phytoplankton growth and zooplankton grazing in the water column or from an increased contribution of diatoms due to the reduction of the sea-ice cover as well as changes in the spatial extent and the timing of the polynya. Although no data are available on their basic life-history traits (e.g. reproduction cycle, seasonal activity rhythms, physiological adaptation to extreme low temperature), our study suggests that the growth of such long-living benthic animals is more resilient over time than expected and well adapted to the variability of PP export to the seabed up to 600 m under the sea surface. Future research is thus needed to understand the underlying mechanisms. It is now well established that global climate change is altering physical settings (currents, water masses, winds, ice coverage, etc.) in the Arctic Ocean. Yet, we do not clearly understand how it will affect high-latitude marine ecosystems. We suggest that climate change will mainly impact food webs dynamics, through cascading effects from primary producers to higher trophic levels. Effects on the benthos depend

on the level of a match-mismatch between phyto- and zooplankton, as well as on the influence of the sea-ice cover through bottom-up regulation of phytoplankton production. Further studies should focus on the fate of the phytoplankton bloom in this particular area at shorter temporal and spatial scales, to better understand variation in the quality and quantity of food reaching the sea floor, and on interactions between physical and biological parameters governing Arctic benthic ecosystems under sea-ice cover.

Data accessibility. We uploaded data in an online data repositories on the Dryad data website with the following DOI: Olivier, Frederic *et al.* (2020), Data related to the MS 'Shells of the bivalve *Astarte moerchi* give new evidence of a strong pelagic-benthic coupling's shift occurring since the late 70s in the NOW Polynya', v2, Dryad, Dataset, https://doi.org/10.5061/dryad.mgqnk98wm.

Authors' contributions. F.O. collected bivalves in the field, conceived, designed and coordinated the study, helped in growth patterns and fatty acid analyses and drafted the manuscript; B.G. produced shell cross-sections, performed all sclero-chronological-chemical as well as fatty acid analyses, participated in all data analyses and helped in drafting the manuscript; J.T. supervised all shell analyses and A.J. help in radiocarbon dating, reader bias assessment and converting trace element and growth increment dataset in time-series; T.M. and R.T. supervised all fatty acid analyses and helped in interpretations of data and drafting the ms; D.D. performed analyses and modelling to provide sea surface annual temperature kinetics and both temporal dynamics and spatial anomaly of SWR and helped in drafting the ms; S.B. performed remote sensing modelling of monthly PP trends and helped in drafting the ms; M.G. provided *in situ* PP data (phytoplankton composition and field incubation measurements) and helped in interpretation of them; L.C. helped in interpretations of all data and critically revised the manuscript and A.M. helped in taxonomical identification of *Astarte* spp. and provided ecological information to interpret data; S.R. helped in radiocarbon dating methods, helped in interpretations of data and critically revised the manuscript; A.-H.O. and J.P. performed Single CPY [53] analyses on increment time-series and J.M. and S.G. performed Multiple CPY [55] analyses on both growth and Ba/Ca times-series; P.A. coordinated field sampling survey, helped in drafting the ms and performed autocorrelation analyses on surface air temperature in electronic supplementary material, S4. All authors helped in revising critically the manuscript and gave final approval for publication and agree to be held accountable for the work performed therein.

Competing interests. We declare we have no competing interests.

Funding. This study was financially supported by ArcticNet (Network of Centres of Excellence of Canada), the Canadian Healthy Oceans Network (CHONe), the Natural Sciences and Engineering Research Council of Canada (NSERC) and Québec-Océan (Fonds de recherche du Québec – Nature et technologies), and by MNHN through a 3-year visiting professorship at ISMER-UQAR to F. Olivier.

Acknowledgements. We thank the Laboratoire de Sclérochronologie des Animaux Aquatiques (LASAA) team for their hospitality and technical assistance with shell sample preparation and analysis. We kindly acknowledge B.R. Schöne (University of Mainz, Institute of Geosciences) for oxygen isotope analysis, C. Bassoullet for trace element analysis, I. Redjah and M. Babin for fatty-acid analysis, and G. Tremblay and S. Lessard for cell identification and enumeration. We thank the crew of the CCGS Amundsen, and V. Roy, A. Fontaine, M. Simard, G. Tremblay, J. Ferland, M. Ardyna, and M. Blais for their technical support during the fieldwork. Thanks to K. Klein, B. Coad and C. McKindsey for linguistic revision and to A. Limoges and JÉ. Tremblay for their comments on the ms. We also thank three anonymous reviewers for their invaluable comments on previous versions of this manuscript.

References

1. ACIA. 2005 *Arctic climate impact assessment*, 1020 pp. New York, NY: Cambridge University Press.
2. Overland J *et al.* 2019 The urgency of Arctic change. *Polar Sci.* **21**, 6–13. (doi:10.1016/j.polar.2018.11.008)
3. Kerr RA. 2012 Ice-free Arctic sea may be years, not decades, away. *Science* **337**, 1591. (doi:10.1126/science.337.6102.1591)
4. Stirling I. 1997 The importance of polynyas, ice edges, and leads to marine mammals and birds. *J. Mar. Syst.* **10**, 9–21. (doi:10.1016/S0924-7963(96)00054-1)
5. Smith WOJ, Barber DG. 2007 Polynyas and Climate Change: A View to the Future. In *Polynyas: windows to the world* (eds WOJ Smith, DG Barber). Amsterdam, The Netherlands: Elsevier Oceanography Series.

6. Barber D, Marsden R, Minnett P, Ingram G, Fortier L. 2001 Physical processes within the North Water (NOW) polynya. *Atmos.-Ocean* **39**, 163–166. (doi:10.1080/07055900.2001.9649673)
7. Dumont D, Gratton Y, Arbetter TE. 2009 Modeling the dynamics of the north water polynya ice bridge. *J. Phys. Oceanogr.* **39**, 1448–1461. (doi:10.1175/2008JPO3965.1)
8. Dumont D, Gratton Y, Arbetter TE. 2010 Modeling wind-driven circulation and landfast ice-edge processes during Polynya Events in northern Baffin Bay. *J. Phys. Oceanogr.* **40**, 1356–1372. (doi:10.1175/2010JPO4292.1)
9. Melling H, Gratton Y, Ingram G. 2001 Ocean circulation within the North Water Polynya of Baffin Bay. *Atmos.-Ocean* **39**, 301–325. (doi:10.1080/07055900.2001.9649683)
10. Mcarthur MA *et al.* 2010 On the use of abiotic surrogates to describe marine benthic biodiversity. *Estuar. Coast. Shelf Sci.* **88**, 21–32. (doi:10.1016/j.ecss.2010.03.003)
11. Snelgrove PVR, Butman CA. 1994 Animal-sediment relationships revisited: cause versus effect. *Oceanogr. Mar. Biol. Annu. Rev.* **32**, 111–177.
12. Ambrose WG, Renaud PE. 1995 Benthic response to water column productivity patterns: evidence for benthic-pelagic coupling in the Northeast Water Polynya. *J. Geophys. Res. Oceans* **100**, 4411–4421. (doi:10.1029/94JC01982)
13. Dunton KH, Goodall JL, Schonberg SV, Grebmeier JM, Maidment DR. 2005 Multi-decadal synthesis of benthic–pelagic coupling in the western arctic: Role of cross-shelf advective processes. *Deep Sea Res. Pt II* **52**, 3462–3477. (doi:10.1016/j.dsr2.2005.09.007)
14. Grebmeier JM, Mcroy CP, Feder HM. 1988 Pelagic-benthic coupling on the shelf of the northern Bering and Chukchi seas. 1. Food supply source and benthic biomass. *Mar. Ecol. Prog. Ser.* **48**, 57–67. (doi:10.3354/meps048057)
15. Piepenburg D, Ambrose Jr WG, Brandt A, Renaud PE, Ahrens MJ, Jensen P. 1997 Benthic community patterns reflect water column processes in the Northeast Water polynya (Greenland). *J. Mar. Syst.* **10**, 467–482. (doi:10.1016/S0924-7963(96)00050-4)
16. Tamelander T, Renaud PE, Hop H, Carroll ML, Ambrose Jr WG, Hobson KA. 2006 Trophic relationships and pelagic–benthic coupling during summer in the Barents Sea Marginal Ice Zone, revealed by stable carbon and nitrogen isotope measurements. *Mar. Ecol. Prog. Ser.* **310**, 33–46. (doi:10.3354/meps310033)
17. Kröncke I, Dippner JW, Heyen H, Zeiss B. 1998 Long-term changes in macrofaunal communities off Norderney (East Frisia, Germany) in relation to climate variability. *Mar. Ecol. Prog. Ser.* **167**, 25–36. (doi:10.1007/BF03042837)
18. Conlan K, Aitken A, Hendrycks E, Mcclelland C, Melling H. 2008 Distribution patterns of Canadian Beaufort Shelf macrobenthos. *J. Mar. Syst.* **74**, 864–886. (doi:10.1016/j.jmarsys.2007.10.002)
19. Feder HM, Naidu AS, Jewett SC, Hameedi JM, Johnson WR, Whitledge TE. 1994 The northeastern Chukchi Sea - benthos-environmental interactions. *Mar. Ecol. Prog. Ser.* **111**, 171–190. (doi:10.3354/meps111171)
20. Sejr MK, Jensen KT, Rysgaard S. 2000 Macrozoobenthic community structure in a high-arctic East Greenland fjord. *Polar Biol.* **23**, 792–801. (doi:10.1007/s003000000154)
21. Richardson CA. 2001 Molluscs as archives of environmental change. *Oceanogr. Mar. Biol. Annu. Rev.* **39**, 103–164.
22. Pannella G, Macclintock C. 1968 Biological and environmental rhythms reflected in molluscan shell growth. *J. Paleontol.* **42**, 64–80. (doi:10.1017/S0022336000061655)
23. Rhoads DC, Pannella G. 1970 The use of molluscan shell growth patterns in ecology and paleoecology. *Lethaia* **3**, 143–161. (doi:10.1111/j.1502-3931.1970.tb01854.x)
24. Jones DS, Arthur MA, Allard DJ. 1989 Sclerochronological records of temperature and growth from shells of *Mercenaria mercenaria* from Narragansett Bay, Rhode Island. *Mar. Biol.* **102**, 225–234. (doi:10.1007/BF00428284)
25. Müller-Lupp T, Bauch H. 2005 Linkage of Arctic atmospheric circulation and Siberian shelf hydrography: a proxy validation using ∂^{18}O records of bivalve shells. *Global Planet. Change* **48**, 175–186. (doi:10.1016/j.gloplacha.2004.12.012)
26. Witbaard R, Duineveld GCA, Dewilde P. 1997 A long-term growth record derived from *Arctica islandica* (Mollusca, Bivalvia) from the Fladen Ground (northern North Sea). *J. Mar. Biol. Assoc. U.K.* **77**, 801–816. (doi:10.1017/S0025315400036201)
27. Schöne BR *et al.* 2003 North Atlantic Oscillation dynamics recorded in shells of a long-lived bivalve mollusk. *Geology* **31**, 1037–1040. (doi:10.1130/G20013.1)

28. Wanamaker AD, Kreutz KJ, Schöne BR, Pettigrew N, Borns HW, Introne DS, Belknap D, Maasch KA, Feindel S. 2008 Coupled North Atlantic slope water forcing on Gulf of Maine temperatures over the past millennium. *Clim. Dyn.* **31**, 183–194. (doi:10.1007/s00382-007-0344-8)
29. Sato SI. 1995 Spawning periodicity and shell microgrowth patterns of the venerid bivalve *Phacosoma japonicum* (Reeve, 1850). *The Veliger* **38**, 61–72.
30. Lutz RA, Rhoads DC. 1980 Growth patterns within the molluscan shell. An overview. In *Skeletal growth and aquatic organisms* (eds DC Rhoads, RA Lutz), pp. 203–254. New York, NY: Plenum Press.
31. Coe WR. 1948 Nutrition, environmental conditions, and growth of marine bivalves mollusks. *J. Mar. Res.* **7**, 586–601. (doi:10.1111/j.1442-9993.1993.tb00438.x)
32. Ambrose WG, Carroll ML, Greenacre M, Thorrold SR, Mcmahon KW. 2006 Variation in *Serripes groenlandicus* (Bivalvia) growth in a Norwegian high-Arctic fjord: evidence for local- and large-scale climatic forcing. *Glob. Change Biol.* **12**, 1595–1607. (doi:10.1111/j.1365-2486.2006.01181.x)
33. Butler PG, Wanamaker Jr AD, Scourse JD, Richardson CA, Reynolds DJ. 2013 Variability of marine climate on the North Icelandic Shelf in a 1357-year proxy archive based on growth increments in the bivalve *Arctica islandica*. *Palaeogeogr. Palaeoclimatol. Palaeoecol.* **373**, 141–151. (doi:10.1016/j.palaeo.2016.08.006)
34. Carroll ML, Ambrose WG, Levin BS, Locke WL, Henkes GA, Hop H, Renaud PE. 2011 Pan-Svalbard growth rate variability and environmental regulation in the Arctic bivalve *Serripes groenlandicus*. *J. Mar. Syst.* **88**, 239–251. (doi:10.1016/j.jmarsys.2011.04.010)
35. Schöne BR. 2003 A 'clam-ring' master-chronology constructed from a short-lived bivalve mollusc from the northern Gulf of California, USA. *Holocene* **13**, 39–49. (doi:10.1191/0959683603hl593rp)
36. Sejr MK, Blicher ME, Rysgaard S. 2009 Sea ice cover affects inter-annual and geographic variation in growth of the Arctic cockle *Clinocardium ciliatum* (Bivalvia) in Greenland. *Mar. Ecol. Prog. Ser.* **389**, 149–158. (doi:10.3354/meps08200)
37. Carroll ML, Johnson BJ, Henkes GA, Mcmahon KW, Voronkov A, Ambrose WG, Denisenko SG. 2009 Bivalves as indicators of environmental variation and potential anthropogenic impacts in the southern Barents Sea. *Mar. Pollut. Bull.* **59**, 193–206. (doi:10.1016/j.marpolbul.2009.02.022.)
38. Goodwin DH, Schöne BR, Dettman DL. 2003 Resolution and fidelity of oxygen isotopes as paleotemperature proxies in bivalve mollusk shells: models and observations. *Palaios* **18**, 110–125. (doi:10.1669/0883-1351(2003)18<110:rafooi>2.0.co;2)
39. Israelson C, Buchardt B, Funder S, Hubberten HW. 1994 Oxygen and carbon isotope composition of Quaternary bivalve shells as a water mass indicator: Last interglacial and Holocene, East Greenland. *Palaeogeogr. Palaeoclimatol. Palaeoecol.* **111**, 119–134. (doi:10.1016/0031-0182(94)90351-4)
40. Lea D, Boyle E. 1989 Barium content of benthic foraminifera controlled by bottom-water composition. *Nature* **338**, 751–753. (doi:10.1038/338751a0)
41. Gillikin DP, Dehairs F, Lorrain A, Steenmans D, Baeyens W, Andre L. 2006 Barium uptake into the shells of the common mussel (*Mytilus edulis*) and the potential for estuarine paleo-chemistry reconstruction. *Geochim. Cosmochim. Acta* **70**, 395–407. (doi:10.1016/j.gca.2005.09.015)
42. Lazareth CE, Vander Putten E, Andre L, Dehairs F. 2003 High-resolution trace element profiles in shells of the mangrove bivalve *Isognomon ephippium*: a record of environmental spatio-temporal variations? *Estuar. Coast. Shelf Sci.* **57**, 1103–1114. (doi:10.1016/S0272-7714(03)00013-1)
43. Marali S, Schöne BR, Mertz-Kraus R, Griffin SM, Wanamaker AD, Matras U, Butler PG. 2017 Ba/Ca ratios in shells of *Arctica islandica* – potential environmental proxy and crossdating tool. *Palaeogeogr. Palaeoclimatol. Palaeoecol.* **465**, 347–361. (doi:10.1016/j.palaeo.2015.12.018)
44. Thébault J, Chauvaud L, L'helguen S, Clavier J, Barats A, Jacquet S, Pécheyran C, Amouroux D. 2009 Barium and molybdenum records in bivalve shells: geochemical proxies for phytoplankton dynamics in coastal environments? *Limnol. Oceanogr.* **54**, 1002–1014. (doi:10.4319/lo.2009.54.3.1002)
45. Roy V, Iken K, Archambault P. 2014 Environmental Drivers of the Canadian Arctic Megabenthic Communities. *PLoS ONE* **9**, e100900. (doi:10.1371/journal.pone.0100900)

46. Torres ME, Zima D, Falkner KK, Macdonald RW, O'brien M, Schöne BR, Siferd T. 2011 Hydrographic changes in Nares Strait (Canadian Arctic Archipelago) in recent decades based on ∂^{18}O profiles of bivalve shells. *Arctic* **64**, 45–58. (doi:10.14430/arctic4079)
47. Bluhm BA, Gradinger R. 2008 Regional variability in food availability for Arctic marine mammals. *Ecol. Appl.* **18**, S77–S96. (doi:10.1890/06-0562.1)
48. Carroll ML, Carroll J. 2003 The Arctic seas. In *Biogeochemistry of marine systems* (eds KD Black, GB Shimmield), pp. 127–156. Oxford, UK: Blackwell Publishing Ltd.
49. Stewart REA, Campana SE, Jones CM, Stewart BE. 2006 Bomb radiocarbon dating calibrates beluga (*Delphinapterus leucas*) age estimates. *Can. J. Zool.* **84**, 1840–1852. (doi:10.1139/Z06-182)
50. Stuiver M, Polach HA. 1977 Discussion: reporting of ^{14}C data. *Radiocarbon* **19**, 355–363. (doi:10.1017/S0033822200003672)
51. Campana SE, Casselman JM, Jones CM. 2008 Bomb radiocarbon chronologies in the Arctic, with implications for the age validation of lake trout (*Salvelinus namaycush*) and other Arctic species. *Can. J. Fish. Aquat. Sci.* **65**, 733–743. (doi:10.1139/F08-012)
52. Campana SE. 2001 Accuracy, precision and quality control in age determination, including a review of the use and abuse of age validation methods. *J. Fish Biol.* **59**, 197–242. (doi:10.1111/j.1095-8649.2001.tb00127.x)
53. Trauth MH. 2015 *MATLAB® recipes for earth sciences fourth edition, supplementary electronic material, hardcover,* XIV, 427 p. Berlin, Germany: Springer.
54. Lavielle M, Moulines E. 2000 Least-squares estimation of an unknown number of shifts in a time series. *J. Time Ser. Anal.* **21**, 33–59. (doi:10.1111/1467-9892.00172)
55. Lavielle M. 2017 See http://sia.webpopix.org/changePoints.html.
56. Epstein S, Buchsbaum R, Lowenstam HA, Urey HC. 1953 Revised carbonate-water isotopic temperature scale. *Geol. Soc. Am. Bull.* **64**, 1315–1325. (doi:10.1130/0016-7606(1953)64[1315:RCITS]2.0.CO;2)
57. Folch J, Lees M, Stanley GHS. 1957 A simple method for the isolation and purification of total lipides from animal tissues. *J. Biol. Chem.* **226**, 497–509.
58. Marty Y, Delaunay F, Moal J, Samain JF. 1992 Changes in the fatty acid composition of *Pecten maximus* (L.) during larval development. *J. Exp. Mar. Biol. Ecol.* **163**, 221–234. (doi:10.1016/0022-0981(92)90051-B)
59. Bélanger S, Babin M, Tremblay JÉ. 2013 Increasing cloudiness in Arctic damps the increase in phytoplankton primary production due to sea ice receding. *Biogeosciences* **10**, 4087–4101. (doi:10.5194/bg-10-4087-2013)
60. Lee YJ *et al.* 2015 An assessment of phytoplankton primary productivity in the Arctic Ocean from satellite ocean color/in situ chlorophyll-*a* based models. *J. Geophys. Res. Oceans* **120**, 6508–6541. (doi:10.1002/2015JC011018)
61. Gosselin M, Levasseur M, Wheeler PA, Horner RA, Booth BC. 1997 New measurements of phytoplankton and ice algal production in the Arctic Ocean. *Deep Sea Res. Pt II* **44**, 1623–1644. (doi:10.1016/S0967-0645(97)00054-4)
62. Knap A, Michaels A, Close A, Ducklow H, Dickson A. 1996 Protocols for the joint global ocean flux study (JGOFS) core measurements. JGOFS, Reprint of the IOC Manuals and Guides No. 29, UNESCO 1994 19. (doi:10013/epic.27912.d001)
63. Klein B *et al.* 2002 Phytoplankton biomass, production and potential export in the North Water. *Deep Sea Res. Pt II* **49**, 4983–5002. (doi:10.1016/S0967-0645(02)00174-1)
64. Ardyna M, Gosselin M, Michel C, Poulin M, Tremblay JÉ. 2011 Environmental forcing of phytoplankton community structure and function in the Canadian High Arctic: contrasting oligotrophic and eutrophic regions. *Mar. Ecol. Prog. Ser.* **442**, 37–57. (doi:10.3354/meps09378)
65. Parsons TR, Maita Y, Lalli CM. 1984 *A manual of chemical and biological methods for seawater analysis*. Toronto: Pergamon Press.
66. Lund JWG, Kipling C, Le Cren ED. 1958 The inverted microscope method of estimating algal numbers and the statistical basis of estimations by counting. *Hydrobiol.* **11**, 143–170. (doi:10.1007/BF00007865)
67. Clarke KR. 1993 Non-parametric multivariate analyses of changes in community structure. *Aust. J. Ecol.* **18**, 117–143.2. (doi:10.1111/j.1442-9993.1993.tb00438.x)
68. Clarke KR, Gorley RN. 2006 *PRIMER v6: user manual/tutorial (plymouth routines in multivariate ecological research)*. Devon, UK: PRIMER-E.

69. Richardson C. 2001 Molluscs as archives of environmental change. *Oceanogr. Mar. Biol. Ann. Rev.* **39**, 103–164.
70. Gröcke DR, Gillikin DP. 2008 Advances in mollusc sclerochronology and sclerochemistry: tools for understanding climate and environment. *Geo-Mar. Lett.* **28**, 265–268. (doi:10.1007/s00367-008-0108-4)
71. Weidman CR, Jones GA. 1993 A shell-derived time history of bomb 14C on Georges Bank and its Labrador Sea implications. *J. Geophys. Res. Oceans* **98**, 14577–14588. (doi:10.1029/93JC00785)
72. Alkire MB. 2010 Differentiating freshwater contributions and their variability to the surface and halocline layers of the Arctic and subarctic seas, 161 p. Dissertation, Oregon State University.
73. Dalsgaard J, John MS, Kattner G, Müller-Navarra D, Hagen W. 2003 Fatty acid trophic markers in the pelagic marine environment. *Adv. Mar. Biol.* **46**, 225–340. (doi:10.1016/s0065-2881(03)46005-7)
74. Søreide JE, Falk-Petersen S, Hegseth EN, Hop H, Carroll ML, Hobson KA, Blachowiak-Samolyk K. 2008 Seasonal feeding strategies of *Calanus* in the high-Arctic Svalbard region. *Deep Sea Res. Pt II* **55**, 2225–2244. (doi:10.1016/j.dsr2.2008.05.024)
75. De Cesare S, Meziane T, Chauvaud L, Richard J, Sejr MK, Thébault J, Winkler G, Olivier F. 2017 Dietary plasticity in the bivalve *Astarte moerchi* revealed by a multimarker study in two Arctic fjords. *Mar. Ecol. Prog. Ser.* **567**, 157–172. (doi:10.3354/meps12035)
76. Gaillard B, Meziane T, Tremblay R, Archambault P, Layton KKS, Martel AL, Olivier F. 2015 Dietary tracers in *Bathyarca glacialis* from contrasting trophic regions in the Canadian Arctic. *Mar. Ecol. Prog. Ser.* **567**, 139–156. (doi:10.3354/meps12036)
77. Grebmeier JM *et al.* 2006 A major ecosystem shift in the northern Bering Sea. *Science* **311**, 1461–1464. (10.1126/science.1121365)
78. Wassmann P, Duarte CM, Agusti S, Sejr MK. 2011 Footprints of climate change in the Arctic marine ecosystem. *Glob. Change Biol.* **17**, 1235–1249. (doi:10.1111/j.1365-2486.2010.02311.x)
79. Blais M, Ardyna M, Gosselin M, Dumont D, Bélanger S, Tremblay JÉ, Gratton Y, Marchese C, Poulin M. 2017 Contrasting interannual changes in phytoplankton productivity and community structure in the coastal Canadian Arctic Ocean. *Limnol. Oceanogr.* **62**, 2480–2497. (doi:10.1002/lno.10581)
80. Arrigo KR, Van Dijken G, Pabi S. 2008 Impact of a shrinking Arctic ice cover on marine primary production. *Geophys. Res. Lett.* **35**, L19603. (doi:10.1029/2008GL035028)
81. Tremblay JÉ, Anderson LG, Matrai P, Coupel P, Bélanger S, Michel C, Reigstad M. 2015 Global and regional drivers of nutrient supply, primary production and CO_2 drawdown in the changing Arctic Ocean. *Prog. Oceanogr.* **139**, 171–196. (doi:10.1016/j.pocean.2015.08.009)
82. Blicher ME, Rysgaard S, Sejr MK. 2007 Growth and production of sea urchin *Strongylocentrotus droebachiensis* in a high-Arctic fjord, and growth along a climatic gradient (64 to 77° N). *Mar. Ecol. Prog. Ser.* **341**, 89–102. (doi:10.3354/meps341075)
83. Marchese C, Albouy C, Tremblay JÉ, Dumont D, D'Ortenzio F, Vissault S, Bélanger S. 2017 Changes in phytoplankton bloom phenology over the North Water (NOW) polynya: a response to changing environmental conditions. *Polar Biol.* **40**, 1721–1737. (doi:10.1007/s00300-017-2095-2)
84. Bergeron M, Tremblay JÉ. 2008 Shifts in biological productivity inferred from nutrient drawdown in the southern Beaufort Sea (2003–2011) and northern Baffin Bay (1997–2011), Canadian Arctic. *Geophys. Res. Lett.* **41**, 3979–3987. (doi:10.1002/2014GL059649)
85. Arrigo KR, van Dijken GL. 2015 Continued increases in Arctic Ocean primary production. *Prog. Oceanogr.* **136**, 60–70. (doi:10.1016/j.pocean.2015.05.002)
86. Johnsen G, Norli M, Moline M, Robbins I, von Quillfeldt C, Sørensen K, Cottier F, Berge J. 2018 The advective origin of an under ice spring bloom in the Arctic Ocean using multiple observational platforms. *Polar Biol.* **41**, 1197–1216. (doi:10.1007/s00300-018-2278-5)
87. Booth BC, Larouche P, Bélanger S, Klein B, Amiel D, Mei ZP. 2002 Dynamics of *Chaetoceros socialis* blooms in the North Water. *Deep Sea Res. Part II Top. Stud. Oceanogr.* **49**, 5003–5025. (doi:10.1016/s0967-0645(02)00175-3)
88. Martin J, Tremblay JÉ, Price N. 2012 Nutritive and photosynthetic ecology of subsurface chlorophyll maxima in Canadian Arctic waters. *Biogeosciences* **9**, 5353–5371. (doi:10.5194/bg-9-5353-2012)

89. Kemp AES, Pike J, Pearce RB, Lange CB. 2000 The 'Fall dump' - A new perspective on the role of a 'shade flora' in the annual cycle of diatom production and export flux. *Deep Sea Res. Part II Top. Stud. Oceanogr.* **9–11**, 2129–2154. (doi:10.1016/S0967-0645(00)00019-9)
90. Cushing DH. 1990 Plankton production and year-class strength in fish populations: an update of the match/mismatch hypothesis. *Adv. Mar. Biol.* **26**, 249–293. (doi:10.1016/S0065-2881(08)60202-3)
91. Leu E, Søreide JE, Hessen DO, Falk-Petersen S, Berge J. 2011 Consequences of changing sea-ice cover for primary and secondary producers in the European Arctic shelf seas: timing, quantity, and quality. *Prog. Oceanogr.* **90**, 18–32. (doi:10.1016/j.pocean.2011.02.004)
92. Søreide JE, Leu E, Berge J, Graeve M, Falk-Petersen S. 2010 Timing of blooms, algal food quality and *Calanus glacialis* reproduction and growth in a changing Arctic. *Glob. Change Biol.* **16**, 3154–3163. (doi:10.1111/j.1365-2486.2010.02175.x)
93. Boetius A *et al.* 2013 Export of Algal Biomass from the Melting Arctic Sea Ice. *Science* **339**, 1430–1432. (doi:10.1126/science.1231346)
94. Kahru M, Brotas V, Manzano-Sarabia M, Mitchell BG. 2011 Are phytoplankton blooms occurring earlier in the Arctic? *Glob. Change Biol.* **17**, 1733–1739. (doi:10.1111/j.1365-2486.2010.02312.x)